IOP Publishing Journal of Physics: Condensed Matter
J. Phys.: Condens. Matter **32** (2020) 244001 (7pp) https://doi.org/10.1088/1361-648X/ab7b1b

Intermediate range structure of amorphous Cu_2GeTe_3: *ab initio* molecular dynamics study

A Koura and F Shimojo

Department of Physics, Kumamoto University, Kumamoto, Japan

E-mail: koura@kumamoto-u.ac.jp

Received 29 October 2019, revised 30 January 2020
Accepted for publication 28 February 2020
Published 20 March 2020

Abstract

We have investigated the intermediate range structure of amorphous Cu_2GeTe_3 based on *ab initio* molecular dynamics simulations. The highest population of ring size is three, which makes the triangle structure. This ring consists of mainly Cu_2Te. Rings may also consist of CuCuCu, Cu_2Ge, and CuGeTe, where approximately 88% of Cu atoms in the system are related with the three-membered ring. The second highest population of ring size is five. Three- and five-membered rings in the amorphous phase originate from six-membered ring in the crystalline phase. This situation can enhance the phase transition between crystalline and amorphous phases. In the phase change process, Cu atoms may diffuse in the amorphous state with changing bonds. The diffusion coefficient of Cu D_{Cu} is estimated to be approximately 0.12×10^{-9} m^2 s^{-1}. Such high diffusion coefficient of Cu atoms is contributed from only 10% of Cu atoms in the amorphous phase.

Keywords: amorphous, phase change material, molecular dynamics, density functional theory, ring structure

(Some figures may appear in colour only in the online journal)

1. Introduction

Phase transition materials, which change rapidly between crystal and amorphous states, attract many scientific interests because of applications for electronic storage devices. One of the famous compositions is $Ge_2Sb_2Te_5$ (GST) [1, 2]. Cu_2GeSe_3 (CGT) alloy is also one of phase transition materials [3, 4]. In order to clarify the phase change mechanism, many experimental [3–11] and theoretical [9, 12, 13] studies on the crystalline and amorphous phases were carried out so far.

It has been reported by the x-ray powder diffraction that the crystalline CGT has an *Imm*2 space group structure consisting of $GeTe_4$ and $CuTe_4$ tetrahedral units, both of which are connected by the corner-sharing [5]. Jóvári *et al* studied the static structure of amorphous CGT using x-ray diffraction measurements (XRD) and the extended x-ray absorption fine structure (EXAFS) measurements, and also performed Reverse Monte Carlo (RMC) simulation [6]. They found that coordination number of Ge and Cu was 4, which were the same that in the crystalline state. However, Ge–Ge and Cu–Cu homo-polar bonds were found in the amorphous state. Kamimura *et al* performed the x-ray absorption fine structure (XAFS) measurements on crystalline and amorphous CGT [7, 8]. This result is in good consistent with the result of amorphous state by XRD and EXAFS [6].

On the other hand, Chen *et al* carried out *ab inito* molecular dynamics (AIMD) simulations to study the local structure of amorphous CGT based on the density functional theory (DFT) using the generalized gradient approximation (GGA) [12]. In this study, it was suggested that the tetrahedral structure consisted of sp^3 hybridization with lone-pair electron of Te and without d of Cu. Skelton *et al* also studied the static structure and reflectance of crystalline and amorphous CGT using AIMD [13]. It was suggested that geometry consisting of tetrahedral units was important for the phase transition. Densification of amorphous is related with the Cu-rich region such as Cu threefold rings. Although they used the local density

approximation as well as GGA functionals, these functional gave almost same structure. In their study, semi-core electrons of Cu and Ge were also taken into account. Kobayashi *et al* studied the electronic structure and transport properties related with phase change phenomena combining hard x-ray spectroscopy and molecular dynamics (MD) based on DFT using PBE0 hybrid functional [9]. They reported that lone-pair electrons of Te and 3d electrons of Cu contributed importantly to the phase transition process. They suggested that the atomic diffusion of Cu occurred in amorphous CGT, and that the diffusion was related with the phase transition between crystalline and amorphous phases. Such diffusion of Cu/Ag in chalcogenide semiconductors has been also discussed based on AIMD simulations [14].

These suggested phase change mechanisms of CGT seems to be different from that of the case of GST. It has been suggested that the crystallization is accompanied by the increase of ABAB squares (A: Ge, Sb; B: Te) [1, 2]. In other words, it was suggested that four-membered ring structure played a key roll in the phase transition. However, such local and/or intermediate range ordering in amorphous CGT is not clear enough.

In this study, we have investigated the static and dynamic properties of amorphous CGT based on AIMD simulations. In order to clarify the intermediate range structure of the amorphous state, we show pair distribution functions, coordination numbers, and the result of ring analysis. The atomic diffusion of Cu atoms is also discussed. Our analysis of local and intermediate range would give better suggestion.

2. Numerical method

The electronic states were calculated using the projector augmented wave (PAW) method [15, 16] within the framework of DFT, in which the GGA was used for the exchange–correlation energy [17]. The plane-wave cutoff energies were 20 and 120 Ry for the electronic pseudo-wave functions and pseudo-charge densities, respectively. Projector functions were generated $3d^{10}4s^{1}4p^{0}$, $4s^{2}4p^{2}4d^{0}$, and $5s^{2}5p^{4}5d^{0}$ for Cu, Ge, and Te, respectively. For telluride materials, it has been suggested by Micoulaut *et al* that taking the dispersion correction into account makes the bond distance and density better even in bulk systems including amorphous phase [18–20]. Therefore, Grimme's empirical correction, DFT-D2 [21], was also employed in this study.

We used a 144-atom system in a cubic supercell with periodic boundary conditions (PBC). Canonical ensemble was employed at the number density $\rho = 0.0385$ Å^{-3}. Temperature was controlled with Nosé–Hoover thermostat technique [22, 23]. Molecular dynamics was performed at the timestep $\Delta t = 2.9$ fs.

In order to obtain the amorphous state, the crystalline structure was prepared as an initial configuration. For removing the dependence of crystal structure, we started the simulation at 4000 K during 4.35 ps. An amorphous state was obtained by cooling step by step from 4000 to 300 K. Furthermore, another amorphous state was also made to average the former and latter. The latter amorphous was prepared with additional 2.9 ps calculation at 4000 K, i.e., 7.25 ps at 4000 K in total. Here after we call the former and latter a1 and a2 amorphous states, respectively. In the cooling process, cooling rates of a1 and a2 states were approximately 2.1 and 2.3×10^{14} K s^{-1}, respectively. Physical quantities of our interest were obtained by averaging 33.4 and 24.7 ps at 300 K for a1 and a2 amorphous states, respectively, after 1.45 ps equilibration.

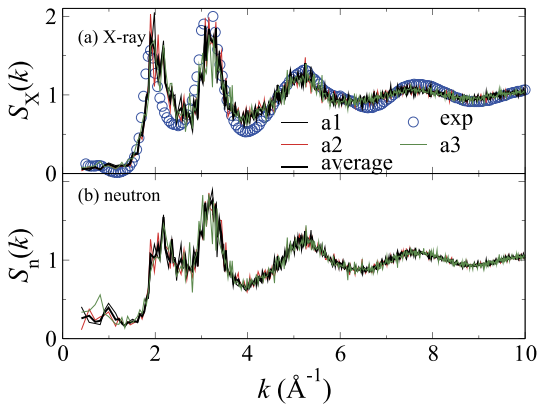

Figure 1. Static structure factors (a) $S_X(k)$ and (b) $S_n(k)$. $S_X(k)$ and $S_n(k)$ were obtained from using the x-ray form factor and the neutron scattering length, respectively. The black and red lines show structure factors of a1 and a2 amorphous states, respectively. The black bold line indicates the average of them. The blue circle shows the result of the experiment [10]. The green line incicates $S_X(k)$ and (b) $S_n(k)$ of a3 amorphous state (see section 3.5).

3. Results and discussion

3.1. Static structure factors

Figure 1 shows the static structure factors using (a) x-ray form factors and (b) neutron scattering length. The black and red lines indicate those of a1 and a2 amorphous states, respectively. The black bold line corresponds to the average of them. Peak and minimum positions of obtained structure factor $S_X(k)$ are in reasonable agreement with the experimental result indicated with blue circle [10].

3.2. Pair distribution functions

The black bold lines in figure 2 indicate the average of total and partial pair distribution functions $g(r)$ and $g_{\alpha\beta}(r)$ of amorphous CGT. Black and red thin lines show those in different amorphous a1 and a2 states, respectively. Left-hand side panels, i.e., figures 2(a)–(d), indicate $g(r)$ and $g_{\alpha\alpha}(r)$, which means partial pair distribution functions between the same type atoms, respectively. Right-hand side panels, figures 2(e)–(g), correspond to $g_{\alpha\beta}(r)$ of hetero-type pairs. The blue dashed vertical lines indicate the half length of supercell.

In figure 2(a), although it looks as if only bold line has been shown, black and red thin lines are also displayed. To distinguish $g(r)$ of a1 and a2 amorphous states easily, the difference between $g(r)$ of a1 state and that of a2 state, $\Delta g(r) = g^{(a1)}(r) - g^{(a2)}(r)$, was shown by pink solid line in figure 2(a). This difference are almost zero except for a small fluctuation at around first peak position. This fact means that total $g(r)$ does not depend on the cooling process. On the other correlation

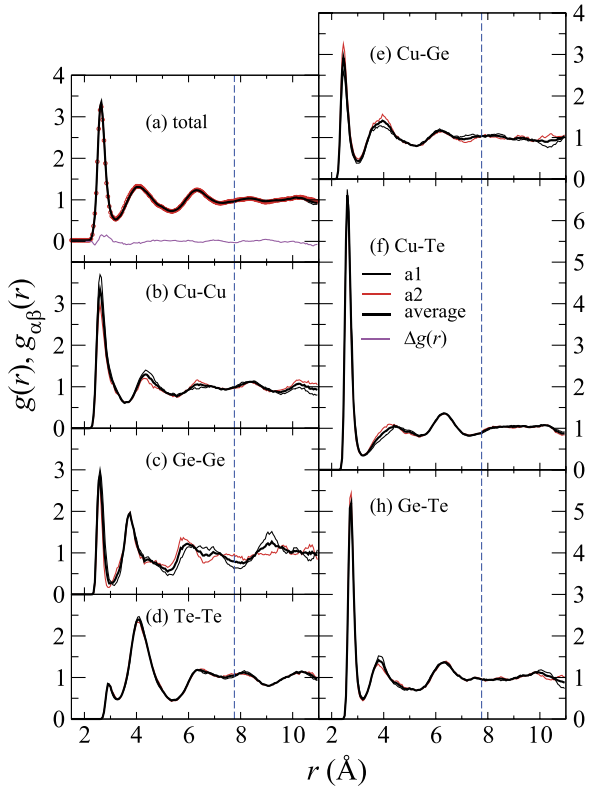

Figure 2. Pair distribution functions $g(r)$ and partial pair distribution functions $g_{\alpha\beta}(r)$ of amorphous Cu_2GeTe_3. Black solid and red dashed lines correspond to a1 and a2 amorphous states, respectively. Black bold line shows the average of them.

functions $g_{\alpha\beta}(r)$, each first peak position of a1 state is almost the same as that of a2 state. However, their heights of the first peaks of $g_{\mathrm{CuCu}}(r)$ and $g_{\mathrm{CuGe}}(r)$ are slightly different between a1 and a2 states. These differences are probably caused by the number of atoms (48 Cu and 24 Ge atoms). Furthermore, $g_{\mathrm{CuCu}}(r)$ has a small shoulder or long tail up to approximately 3.5 Å. This fact supposes the large atomic fluctuation of Cu atoms (see section 3.4).

Peak positions of first peaks of $g_{\mathrm{CuCu}}(r)$ and $g_{\mathrm{GeGe}}(r)$ are 2.61 and 2.59 Å, respectively. The other positions of first peaks listed in table 1 have a similar value except for that of $g_{\mathrm{TeTe}}(r)$, which is slightly longer than those of others. Additionally, our $g_{\mathrm{TeTe}}(r)$ has a similar profile of $g_{\mathrm{TeTe}}(r)$ obtained by Chen *et al* (see their supplementary material [12]). However, the height of the first peak of $g_{\mathrm{TeTe}}(r)$ of ours is rather lower than that in other experimental [6, 10, 11] and theoretical results [13]. This discrepancy is probably caused by the difficulty to determine the constraint, e.g., cutoff distance and bond angles, in the RMC simulation [6, 10, 11].

In $8 - N$ rule, the average coordination number should be 4 in this system. In other results, although the coordination numbers depend on each cutoff distance, total $N = 4.79$ [10], 4.08 [6], and 5.06 [13] were reported. Obtained average coordination numbers N, N_α, and $N_{\alpha\beta}$ of ours are listed in table 1. To estimate coordination numbers, the cutoff distance $r_c = 3.2$ Å was adopted. This distance corresponds to the position of first minimum of $g(r)$. As discussed by Skelton *et al* [13], our coordination number of Cu, N_{Cu}, is also larger than 4. In figure 3,

Table 1. Average peak positions, $r^{\mathrm{p}}_{\alpha\beta}$, of first peak of pair distribution functions and average coordination numbers N, N_α, and $N_{\alpha\beta}$. The coordination numbers were defined using the cutoff distance $r_c = 3.2$ Å.

Atom	$r^{\mathrm{p}}_{\alpha\beta}$ (Å)	$N, N_\alpha, N_{\alpha\beta}$
Total	2.64	4.66
Cu		5.96
Ge		4.59
Te		3.82
Cu–Cu	2.61	1.94
Ge–Ge	2.59	0.52
Te–Te	2.91	0.62
Cu–Ge	2.45	0.62
Ge–Cu		1.25
Cu–Te	2.61	3.39
Te–Cu		2.26
Ge–Te	2.73	2.83
Te–Ge		0.94

which shows distributions of coordination number $d_{\alpha\beta}(N)$, Cu atoms may have large coordination number to other Cu atoms up to 5, where N_{CuCu} reaches 1.94. These facts mean that there clearly exists Cu-rich region. On the other hand, the average coordination number of Te, N_{TeTe} is smaller than results from RMC [6, 10], and is in good agreement with results from AIMD [12, 13]. Some distributions related with Cu and Ge, e.g., $d_{\mathrm{CuCu}}(N = 1)$, $d_{\mathrm{GeCu}}(N = 0)$, $d_{\mathrm{GeCu}}(N = 3)$, of a1 amorphous state (black line) are slightly different from those of a2 state (red line). This reason is probably the number of atoms. Althogh for Cu–Te, a1 and a2 states seems to have different peaks of $d_{\mathrm{CuTe}}(N = 4)$ and $d_{\mathrm{CuTe}}(N = 3)$, respectively, the averaged line (bold line with circle) would be more similar to the bulk amorphous CGT. The other distributions $d_{\alpha\beta}(N)$ of a1 amorphous state are in good agreement with those of a2 states.

3.3. Ring structure

In order to investigate the intermediate structure, it is a suitable method to employ the ring analysis shown in figure 4(a). The cutoff distance to define the bond is $r_c = 3.2$ Å (see figure 5). Black and red lines correspond to populations of M-membered ring $P(M)$ in a1 and a2 amorphous phases, respectively. The result drawn with the green line is discussed in the section 3.5. In our study, the ring size of the highest population is 3, which corresponds to experimental [10, 11] and theoretical [12] results. This highest population of ring size 3 in amorphous CGT is rather different from that in amorphous GST [1], where the four-membered ring is the highest population. On the ring size of the next highest population, however, there is a difference between the results by Chen *et al* [12] and Stellhorn *et al* [10, 11].

Chen *et al* reported that next highest populations were 5 and 7, and 6 is rather less [12]. On the other hand, ring sizes of the second highest in experimental [10, 11] and our study were 6 and 5, respectively. From the viewpoint of the phase transition between crystalline and amorphous phases, it would be

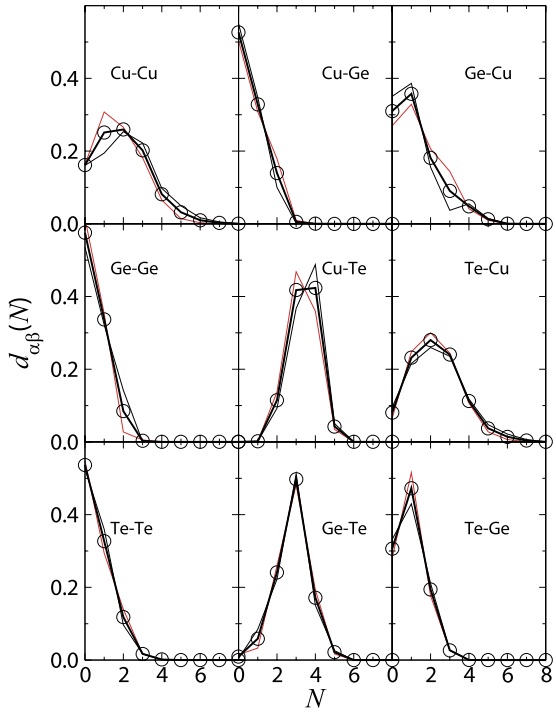

Figure 3. Distribution $d_{\alpha\beta}(N)$ of coordination numbers $N_{\alpha\beta}$. Bonds are defined using the cutoff distance $r_c = 3.2$ Å. Black and red thin lines correspond to $d_{\alpha\beta}(N)$ of a1 and a2 states, respectively. Black bold line with circle shows the average of them.

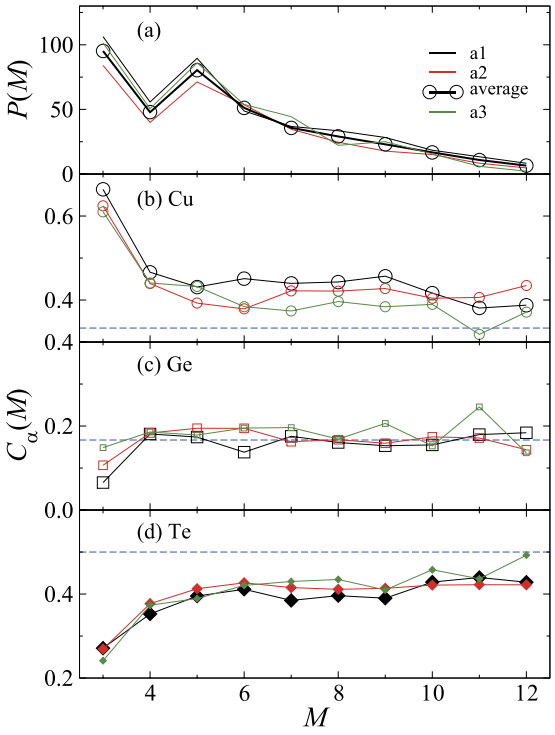

Figure 4. (a) Population of ring sizes $P(M)$. Black, red, and green solid lines show $P(M)$ of a1, a2, and a3 amorphous states, respectively. Black bold line with open circles indicates the average of results of a1 and a2 states. (b)–(d) Component ratio $C_\alpha(M)$ in M-membered ring. Black, red, and green correspond to a1, a2, and a3 amorphous states, respectively. Ring is defined using the cutoff distance $r_c = 3.2$ Å. Blue dashed line indicates the concentration of Cu, Ge, and Te atoms in the amorphous Cu_2GeTe_3.

reasonable that the six-membered ring in the crystalline state changes to three- and five-membered rings in the amorphous phase schematically by disordering. It may enhance the fast phase transition. However, too low population of ring size 6 is rather strange because the melt-quench method is adopted, therefore the ring size 6, which is similar to the crystalline state, should exist more in the amorphous phase. On the other hand, our result, where many six-membered rings coexist in the amorphous, looks better than the previous calculation [12]. This difference of the results would be caused by several reasons, which are system size, dispersion correction, simulation time at 300 K. 90 atoms in a cubic supercell is rather small to consider the intermediate range structure. Indeed, the largest size of ring was 8 in their work [12]. As examples of rings, snapshots of six- and twelve-membered rings are shown in figure 5. In these figures, blue, pink, and red balls correspond to Cu, Ge, and Te atoms, respectively. Blue bold bonds mean each ring. All bonds in these figures are drawn using $r_c = 3.2$ Å. For references, distances between labelled atoms are: (a) Te1–Cu2 (4.9 Å) and Te2–Cu1 (4.6 Å), (b) Te3–Te4 (10.0 Å) and Te3–Te5 (10.1 Å). We have confirmed the existence of a few twelve-membered rings, such large sized rings might be affected by PBC, e.g., $M > 10$ in reference to the atomic distance mentioned above.

Figures 4(b)–(d) show the component ratio of M-membered ring $C_\alpha(M)$, which is defined as the following relation:

$$C_\alpha(M) = \frac{n_\alpha^{(M)}}{M},$$

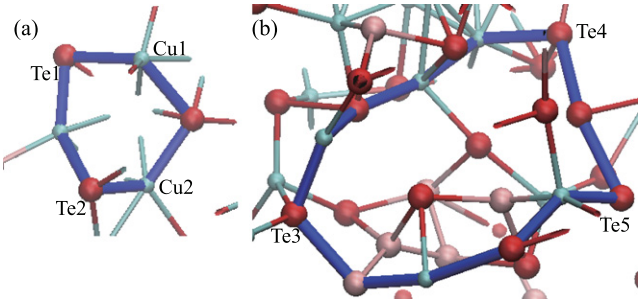

Figure 5. Snapshots of (a) six-membered ring and (b) twelve-membered ring. Blue, pink, and red balls correspond to Cu, Ge, and Te atoms, respectively. Blue bold bonds mean one of rings. Bonds are drawn using the cutoff distance $r_c = 3.2$ Å.

where $n_\alpha^{(M)}$ is the time-averaged number of α-type atoms consisting of M-membered ring. Numbers $n_\alpha^{(M)}$ were counted in each ring. Black, red, and green lines correspond to $C_\alpha(M)$ in a1, a2, and a3 states, respectively. Blue dashed line indicates the concentration of Cu, Ge, and Te atoms in the amorphous Cu_2GeTe_3. In any ring size M, $C_{Cu}(M)$ is higher than the concentration of Cu (0.333) in amorphous CGT and $C_{Te}(M)$ is lower than that of Te (0.500). Indeed, a Cu-rich six-membered ring is shown in figure 5(a).

Table 2. Average population of atoms in three-membered rings $C_\alpha(3)$ and p_α.

Atom	$C_\alpha(3)$	p_α	Concentration
Cu	0.625	0.878	0.333
Ge	0.107	0.474	0.167
Te	0.269	0.512	0.500

Furthermore, three-membered ring consists of approximately 65% of Cu, 7% of Ge, and 28% of Te atoms. Details of the three-membered ring are Cu_2Te [62.3%], CuGeTe [14.5%], CuCuCu [11.9%], Cu_2Ge [8.8%], and $CuTe_2$ [2.8%]. $CuGe_2$, $GeTe_2$, and Ge_2Te are less than approximately 1%. GeGeGe and TeTeTe rings are rarely found in spite of using a little long cutoff distance comparing with positions of their first minimum of $g_{\mathrm{GeGe}}(r)$ and $g_{\mathrm{TeTe}}(r)$.

Focusing on the contribution of atomic species to the three-membered ring, there is clear deviation from the concentration of each species in the material as listed in table 2. The contribution is defined as the participation ratio p_α,

$$p_\alpha = \frac{n'^{(3)}_\alpha}{n_\alpha}$$

where n_α is the number of α-type atoms in the system. Although $n'^{(3)}_\alpha$ is also the number of α-type atoms consisting of a three-membered ring, which is different from $n^{(M=3)}_\alpha$, $n'^{(3)}_\alpha$ is counted not in each ring but in the whole system. The component ratio of three-membered ring $C_\alpha(3)$ is also listed in table 2. On the three-membered ring, although $C^{(3)}_{\mathrm{Te}}$ is rather lower than the concentration of Te in the alloy, p_{Te} is almost same as the concentration of Te. On Ge atoms, $C_{\mathrm{Ge}}(3)$ is also lower than the concentration of Ge, however, p_{Ge} is three times higher than the concentration of Ge. On the other hand, both $C_{\mathrm{Cu}}(3)$ and p_{Cu} are higher than the concentration of Cu. When the six-membered ring in the crystalline state is distorted by the phase transition, it is considered that three types of 3 + 5 rings can appear in the amorphous phase geometrically. They are CuTeCu (Cu_2Te) + CuTeGeTeCu, CuTeGe (CuGeTe) + GeTeCuTeCu, and TeCuTe ($CuTe_2$) + TeCuTeGeTe rings. In amorphous phase, as mentioned above, Cu_2Te and CuGeTe rings exist 62.3 and 14.5%, respectively. However, $CuTe_2$ ring only exists 2.8%, i.e., the last type of 3 + 5 ring is minor than CuCuCu ring. This is also shown in $C_{\mathrm{Te}}(3) = 0.269$. Hence, Cu-rich region appears in the amorphous phase.

3.4. Atomic diffusion of Cu atoms

As described above, the slope of the first peak of $g_{\mathrm{CuCu}}(r)$ and other properties suggest an atomic large fluctuation or diffusion of Cu atoms. The atomic diffusion of Cu atoms was also suggested in the recent study [9]. In figures 6(a) and (b), square displacements $|\boldsymbol{r}_i(t) - \boldsymbol{r}_i(0)|^2$ of ith Cu atoms in a1 and a2 amorphous states are shown, respectively. For comparison, those of some Ge and Te atoms are also shown in figures 6(c) and (d), respectively.

In the superionic material case, for example, Cu or Ag atoms migrate in superionic phase of CuI or Ag_2Se, then, mean square displacements of them have profiles like linear as a function of t. Although amorphous CGT is not considered as a superionic material, approximately 10% of Cu atoms have such large square displacements in this simulation. Here, the diffusion coefficient of Cu, D_{Cu}, can be estimated from the slope of mean square displacement of Cu as approximately 0.12×10^{-9} m^2 s^{-1}.

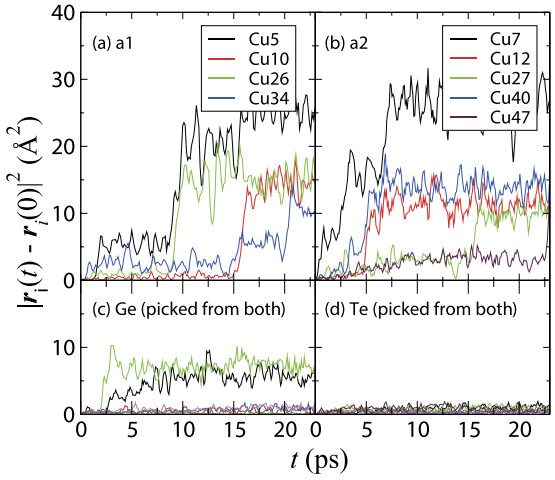

Figure 6. Square displacements of ith atom. Panels (c) and (d) show square displacements of several Ge and Te atoms in a1 and a2 states.

When the phase transition from amorphous to crystalline phases occurs, CuTeCuTeGeTe six-membered rings must appear in the crystal. To make the six-membered rings, Cu_2Te and CuGeTe three-membered rings in amorphous are reasonable. Although $GeTe_2$ ring exists only 2.8%, it is also possible. While, inconvenient configurations to fast phase transition are CuCuCu and Cu_2Ge, and the sum of them is 20.7% in three-membered rings. Indeed, p_{Cu} and p_{Ge} are higher than p_{Te}, such Cu-rich condition is considered as a kind of defect. In order to solve the defect, Cu atoms would migrate to different sites. Kobayashi *et al* mentioned that the diffusion process of Cu atoms was considered as a bottleneck for the reversibility and speed of the phase change process [9]. However, it is suggested that the diffusion of Cu is not a bottleneck but makes the lifetime of amorphous short.

3.5. Dependence of initial configuration and cooling rate

In order to take dependence of initial configuration and cooling rate into account carefully, we carried out another short simulation. This short simulation was started from the random initial configuration, not crystal structure. At first, to obtain liquid state, we annealed it at 4000 K with timestep $\Delta t = 0.96$ fs during 1.44 ps (1500 step). In this liquid state, the total and partial pair distribution functions became similar to those started from the crystalline state soon. Then, a new amorphous state was obtained with quenching from 4000 to 300 K suddenly, i.e., estimated cooling rate was about 10^{18} K s^{-1}. Finally, the simulation at 300 K was performed with timestep $\Delta t = 2.9$ fs during 7.25 ps (2500 step). We call the new amorphous state a3 amorphous state. Physical quantities of a3 amorphous state were obtained by averaging the last 5.8 ps (2000 step).

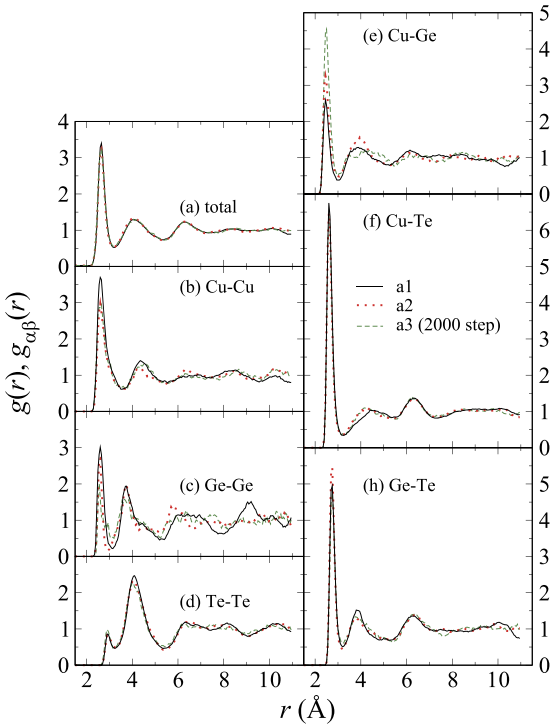

Figure 7. Pair distribution functions $g(r)$ and partial pair distribution functions $g_{\alpha\beta}(r)$ of amorphous Cu_2GeTe_3. Black solid and red dashed lines correspond to a1 and a2 amorphous states, respectively. The green dashed line shows pair distribution functions of a3 amorphous state.

Obtained structure factors $S_X(k)$ and $S_n(k)$ of a3 amorphous state are shown in figure 1 with green line. In spite of the short time averaging, they are in reasonable agreement with those of a1 and a2 states. In the point of view of total pair distribution function $g(r)$ shown in figure 7(a), $g(r)$ of a3 amorphous state drawn with a green dashed line is in good agreement with those of a1 and a2 states. Although the range longer than approximately 7.8 Å would be affected with the periodic boundary condition, $g(r)$ is similar to each other. On partial pair distribution functions $g_{\alpha\beta}(r)$ shown in figures 7(b)–(g), profiles, peak positions and their heights of $g_{\alpha\beta}(r)$ of a3 state are basically similar to those of a1 and a2 states. However, heights of first peaks of $g_{GeGe}(r)$ and $g_{CuGe}(r)$ of a3 state are lower and higher than those of the other states, respectively. In the ring analysis shown in figure 4, the profile of $P(M)$ of a3 state (green line) is also similar to those of a1 and a2 amorphous states. While, $C_{Cu}(M)$ and $C_{Ge}(M)$ of a3 state are slightly different from those of a1 and a2 states. Such differences of $g_{GeGe}(r)$, $g_{CuGe}(r)$, $C_{Ge}(M)$, and $C_{Cu}(M)$ would be caused by number of Cu and Ge atoms rather than the initial configuration or cooling rate.

These facts mean that if CGT is well annealed at high temperature, the structure of amorphous CGT does not depend on the initial configuration and cooling rate so much, although the cooling rate is rather fast comparing with experiments.

4. Conclusion

We have investigated the intermediate range structure of amorphous Cu_2GeTe_3 based on AIMD simulations. The highest population of ring size is 3, which makes the triangle structure. This ring consists of mainly Cu_2Te. Rings may also consist of CuCuCu, Cu_2Ge, and CuGeTe, where approximately 88% of Cu atoms in the system are related with the three-membered ring. The second highest population of ring size is 5. Three- and five-membered rings in the amorphous phase originate from six-membered rings in the crystalline phase. This situation can enhance the phase transition between crystalline and amorphous phases. In the phase change process, Cu atoms may diffuse in the amorphous state with changing bonds. The diffusion coefficient of Cu D_{Cu} is estimated to be approximately 0.12×10^{-9} m^2 s^{-1}. Such high D_{Cu} is contributed from only 10% of Cu atoms in the amorphous phase.

Acknowledgments

This study was supported by JSPS KAKENHI Grant Number 16K05478, JST CREST Grant Number JPMJCR1861 and JPMJCR18I2, Japan. The authors thank the Supercomputer Center, the Institute for Solid State Physics, University of Tokyo for the use of the facilities. This work has also been done using the facilities of the Research Institute for Information Technology, Kyushu University. The authors thank Dr J R Stellhorn for providing the experimental data and useful discussion.

ORCID iDs

A Koura https://orcid.org/0000-0003-3870-7346

References

[1] Akola J and Jones R O 2008 Density functional study of amorphous, liquid and crystalline Ge(2)Sb(2)Te(5): homopolar bonds and/or ab alternation? *J. Phys.: Condens. Matter* **20** 465103
[2] Kalikka J, Akola J and Jones R O 2014 Simulation of crystallization in $Ge_2Sb_2Te_5$: a memory effect in the canonical phase-change material *Phys. Rev.* B **90** 184109
[3] Sutou Y, Kamada T, Sumiya M, Saito Y and Koike J 2012 Crystallization process and thermal stability of $Ge_1Cu_2Te_3$ amorphous thin films for use as phase change materials *Acta Mater.* **60** 872–80
[4] Kamada T, Sutou Y, Sumiya M, Saito Y and Koike J 2012 Crystallization and electrical characteristics of $Ge_1Cu_2Te_3$ films for phase change random access memory *Thin Solid Films* **520** 4389–93
[5] Delgado G E, Mora A J, Pirela M, Velásquez-Velásquez A, Villarreal M and Fernández B J 2004 Structural refinement of the ternary chalcogenide compound Cu_2GeTe_3 by x-ray powder diffraction *Phys. Status Solidi* A **201** 2900–2904
[6] Jóvári P, Sutou Y, Kaban I, Saito Y and Koike J 2013 Fourfold coordinated Te atoms in amorphous $GeCu_2Te_3$ phase change material *Scr. Mater.* **68** 122–5
[7] Kamimura K, Kimura K, Hosokawa S, Happo N, Ikemoto H, Sutou Y, Shindo S, Saito Y and Koike J 2016 XAFS analysis of crystal $GeCu_2Te_3$ phase change material *Z. Phys. Chem.* **230** 433
[8] Kamimura K, Hosokawa S, Happo N, Ikemoto H, Sutou Y, Shindo S, Saito Y and Koike J 2016 XAFS analysis on

amorphous and crystalline new phase change material $GeCu_2Te_3$ *J. Optoelectron Adv. M.* **18** 248–53

[9] Kobayashi K, Skelton J M, Saito Y, Shindo S, Kobata M, Paul F, Kolobov A V, Elliott S, Ando D and Sutou Y 2018 Understanding the fast phase-change mechanism of tetrahedrally bonded Cu_2GeTe_3: comprehensive analyses of electronic structure and transport phenomena *Phys. Rev.* B **97** 195105

[10] Stellhorn J R, Paulus B, Hosokawa S, Pilgrim W-C, Boudet N, Blanc N and Sutou Y 2019 Structure of amorphous Cu_2GeTe_3 and a model for its fast phase-change mechanism (arXiv:1908.07297) [cond-mat.mtrl-sci]

[11] Stellhorn J R, Hosokawa S and Kohara S 2020 Local- and intermediate-range structures on ordinal and exotic phase-change materials by anomalous x-ray scattering *Anal. Sci.* **36** 5–16

[12] Chen N-K, Li X-B, Wang X-P, Xia M-J, Xie S-Y, Wang H-Y, Song Z, Zhang S and Sun H-B 2015 Origin of high thermal stability of amorphous $Ge_1Cu_2Te_3$ alloy: a significant Cu-bonding reconfiguration modulated by Te lone-pair electrons for crystallization *Acta Mater.* **90** 88–93

[13] Skelton J M, Kobayashi K, Sutou Y and Elliott S R 2013 Origin of the unusual reflectance and density contrasts in the phase-change material Cu_2GeTe_3 *Appl. Phys. Lett.* **102** 224105

[14] Ma J and Wei S-H 2013 Origin of novel diffusions of Cu and Ag in semiconductors: the case of CdTe *Phys. Rev. Lett.* **110** 235901

[15] Blöchl P E 1994 Projector augmented-wave method *Phys. Rev.* B **50** 17953–79

[16] Kresse G and Joubert D 1999 From ultrasoft pseudopotentials to the projector augmented-wave method *Phys. Rev.* B **59** 1758–75

[17] Perdew J P, Burke K and Ernzerhof M 1996 Generalized gradient approximation made simple *Phys. Rev. Lett.* **77** 3865–8

[18] Micoulaut M 2013 Communication: van der Waals corrections for an improved structural description of telluride based materials *J. Chem. Phys.* **138** 061103

[19] Micoulaut M, Coulet M-V, Piarristeguy A, Johnson M R, Cuello G J, Bichara C, Raty J-Y, Flores-Ruiz H and Pradel A 2014 Effect of concentration in Ge-Te liquids: a combined density functional and neutron scattering study *Phys. Rev.* B **89** 174205

[20] Micoulaut M, Piarristeguy A, Flores-Ruiz H and Pradel A 2017 Towards accurate models for amorphous gete: crucial effect of dispersive van der waals corrections on the structural properties involved in the phase-change mechanism *Phys. Rev.* B **96** 184204

[21] Grimme S 2006 Semiempirical GGA type density functional constructed with a long-range dispersion correction *J. Comput. Chem.* **27** 1787–99

[22] Nosé S 1984 A unified formulation of the constant temperature molecular dynamics methods *J. Chem. Phys.* **81** 511–9

[23] Hoover W G 1985 Canonical dynamics: equilibrium phase-space distributions *Phys. Rev.* A **31** 1695–7